

# Optimization and Design of Multi-ring Pole Pieces for Small-sized Permanent Magnetic Resonance Imaging Magnet

Yi-Yuan Cheng<sup>1</sup>, Tao Hai<sup>1</sup>, Yang-Bing Zheng<sup>1</sup>, Bao-Lei Li<sup>2</sup>, and Ling Xia<sup>3</sup>

<sup>1</sup>Department of Mechanical and Electrical Engineering  
Nanyang Normal University, Nanyang, 473061, China  
chengyy850@gmail.com, nytcht@163.com, zhengyb505@163.com

<sup>2</sup>Department of Physics and Electrical Engineering  
Nanyang Normal University, Nanyang, 473061, China  
bl\_li@qq.com

<sup>3</sup>Department of Biomedical Engineering  
Zhejiang University, Hangzhou, 310027, China  
xialing@zju.edu.cn

**Abstract** — In magnetic resonance imaging (MRI) system, the main magnet creates a static magnetic field, which largely determines the final imaging quality. Pole pieces of pure-iron are commonly used to improve the field homogeneity in the imaging region. In this work, we attempt to design a novel configuration of multi-ring pole pieces for a small animal MRI system. Based on the model of a small H-type permanent magnet, the magnetic field is calculated using the finite element method, which considers the nonlinearity of the ferromagnetic materials. The pole piece was designed with the particle swarm optimization (PSO) algorithm. The results show that, the optimal multi-ring pole pieces can effectively reduce the uniformity about 10-20 ppm ( $10^{-6}$ ), with a better performance compared with the flat and traditional one-ring pole piece configuration.

**Index Terms** — Multi-ring pole pieces, nonlinear optimization, particle swarm optimization, permanent MRI magnet.

## I. INTRODUCTION

Nowadays, magnetic resonance imaging (MRI) has become one of the most powerful and important noninvasive diagnostic tools for medical imaging. MRI requires a strong and uniform magnetic field in the imaging region [1-2] which is generated by permanent, resistive or superconducting magnets. Recently, permanent magnets have gained widespread popularity in both clinical applications and biomedical research studies, especially for small animal MRI researches [3-4], due to the low weight, cost and less consumption of electricity, coolant water, and no expensive liquid Helium [5-6].

In a permanent MRI system, the static magnetic

field is generated by permanent ferromagnetic materials, and the well-known widespread end-effect can cause a non-uniform magnetic field distribution and therefore affects the imaging quality [7-8]. Shimming is used prior to the operation of the magnet to improve the homogeneity of the magnetic field. The pole piece made of pure iron can be used to adjust the uniformity of the magnetization characteristic of the permanent material blocks, and special design of shapes of the pole piece can help to improve the field homogeneity in the imaging volume [9]. Previously, several studies have discussed the design and optimization of the shape of the pole piece [10-15] in the standard MRI systems. In these designs, the final pole piece geometry is usually with one shimming ring or curved surface. The pole piece with one shimming ring may offer limited capability in improving the field homogeneity. And in paper [12], regular pole pieces with a smoothly-varying radial profile curved surface offer much better performance in shimming the magnetic field. However, these types of configurations with curved surface are usually difficult to manufacture. In this work, we proposed to design simple, novel configurations with multi-ring pole pieces to improve the uniformity of the magnetic field, and applied in a small-sized permanent MRI system.

The design of pole piece in the MRI magnet involves a nonlinear optimization procedure due to the nonlinear characteristic of the ferromagnetic materials, which is the non-convex problem with multi-pole points. In previous studies [12-14], conventional optimization methods such as the steepest descent method were used. These methods have advantages in efficiency, but it searches for the optimal solution along the direction of the gradient and the solution has a great relationship

with the choice of initial value, that might be just local minimums and it is suitable for convex problems. Particle swarm optimization (PSO) [16] algorithm is one of the latest developed intelligence and global optimization methods, which is used in this paper. It has a number of advantages [17-18] including its relatively simple algorithm structure, easy implementation, computational efficiency and immediate applicability to practical problems.

In this work, we take a small H-type permanent magnet for small animal MRI researches as our model; during the design of pole pieces, the magnetic field analysis is performed by the commercial finite element method (FEM) package ANSYS 14.0. Using the developed nonlinear optimization schemes, a number of novel designs of the multi-ring pole pieces have been proposed and discussed.

**II. MODEL AND METHOD**

**A. Permanent magnet model**

As shown in Fig. 1, a small H-type permanent magnet with static magnetic flux density of 0.5 T, and the homogeneous region of a 60 mm diameter sphere volume (DSV) in the center is considered here, which is the effective imaging region.

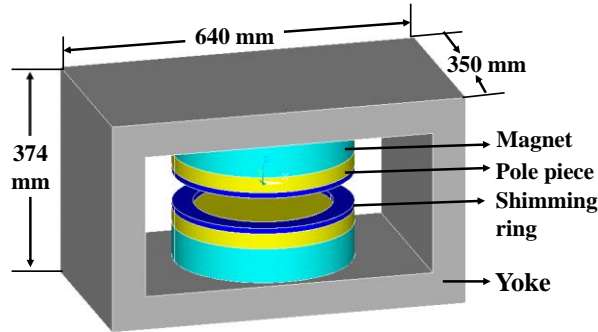


Fig. 1. Construction of the H-type MRI magnet.

The construction of the permanent magnet consists of magnets, pole pieces, shimming rings and the yoke. The single magnet pole made of Nd-Fe-B material (N40) is with 320 mm diameter and 62 mm height, and the air gap between two pole pieces is 75 mm for small animal MRI experiments. The yoke of A3 steel is with 60 mm thickness, and the dimensions have been shown in Fig. 1. The pole pieces with 27.5 mm height and shimming rings made of DT4 pure iron on the surface of magnets are used to improve the uniformity of the magnetic field.

**B. The design of multi-ring pole piece**

The pole piece is made of pure iron on the surface of the magnet. When the surface of the pole piece is flat and the magnetic flux in the air gap is uneven like the drum; this effect, called the end-effect, is shown in Fig.

2 (a). If the shape of the pole piece is designed properly, then the flux in the air gap is no longer outside the drum, accordingly, the central magnetic field becomes uniform, as shown in Fig. 2 (b). In a small permanent magnet, the effect is more serious because a relatively larger imaging area will be formed for such a small sized magnet. The shape of the pole piece plays an important role in improving the field homogeneity in the imaging volume, which is technically more challenging to design.

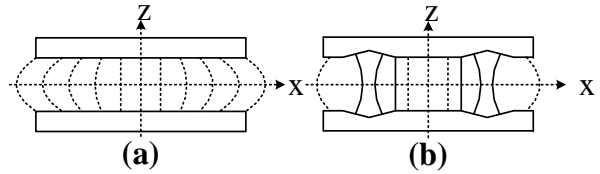


Fig. 2. Magnetic flux distribution. (a) The end-effect; (b) change the shape of pole piece.

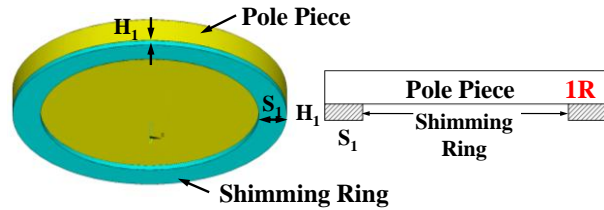


Fig. 3. The pole piece model with a shimming ring and the cross-section.

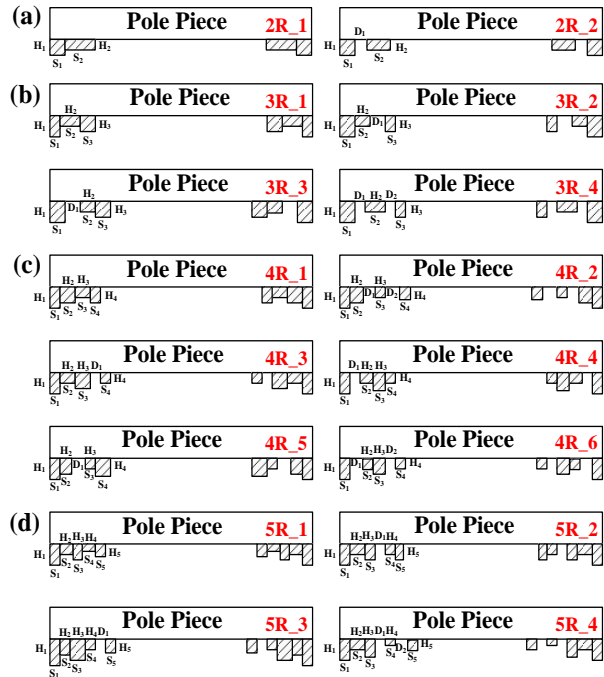


Fig. 4. The cross-section of multi-ring. (a) Two rings; (b) three rings; (c) four rings; (d) five rings.

A shimming ring of the rectangular cross-section is commonly used to adjust the field uniformity in the imaging area, as shown in Fig. 3. A series of rings will be taken into consideration in our work; here, the maximum number of rings we considered is five, because too many rings can make the structure complicated, and difficult to model and manufacture. The cross-sections of rings to be designed in this paper are shown in Fig. 3 and Fig. 4, and each structure is named as the figures, such as 1R, 2R, 3R meaning the number of the rings used in the design and the suffix '\_1', '\_2'... meaning the different arrangement of the rings and the gap. Meanwhile, the flat pole piece without a shimming ring is named NR.

### C. Magnetic field calculation

The finite element method (FEM) is widely used for the calculation of the magnetic fields. In the analysis of the static magnetic field, the finite element equation is described by the vector magnetic potential  $A$  as:

$$B = \nabla \times A. \quad (1)$$

Under the constraint conditions of  $\nabla \cdot A = 0$ ,  $A$  satisfies the boundary value problem, that is:

$$\begin{cases} \nabla^2 A = -\mu J & \text{in the field of } V \\ A|_S = C & \text{on the boundary of } S \end{cases}, \quad (2)$$

where  $\mu$  is the permeability,  $J$  is the incentive current density and  $C$  is the boundary condition.

In this paper, the 3D FEM analysis of the permanent magnet has been carried out by using the commercial general software ANSYS (version 14.0, www.ansys.com). Due to symmetry of the magnet model, a half model is considered. Because the plane of symmetry is perpendicular to the magnetic field lines of the model, the boundary conditions in the plane of symmetry don't need to be handled in ANSYS. The conditions of air field boundary in a long distance are set to zero flux, which is 5 times as the height, the length and width of the whole magnet model respectively. The ferromagnetic material and the air gap are both calculated in the magnet model, so we choose solid 117 type element in ANSYS which adopt the edge-based FEM. The model is divided by free tetrahedral mesh. According to the practical experience of meshing, the components we concern about or the components with the larger changed magnetic fields need be divided into smaller grids, so a fine mesh is used in the DSV region, the pole piece and shimming rings. In addition, the relatively unconcerned components, such as the magnet, the yoke and the outside air part with the relatively small changed magnetic fields, are meshed by a slightly coarse grid.

The model is partitioned into approximately 55000 tetrahedron elements, as shown in Fig. 5 (a), with a maximum element size of 10 mm specified over a 60 mm DSV. There are 348 volume elements and 278 nodes in the DSV as shown in Fig. 5 (b), and the magnetic

flux density of each element is used to calculate the uniformity of DSV. The magnet pole is partitioned into 459 elements with 347 nodes, and the pole piece has 2501 elements and 1506 nodes. The yoke are meshed by a slightly coarse grid with 475 elements and 280 nodes.

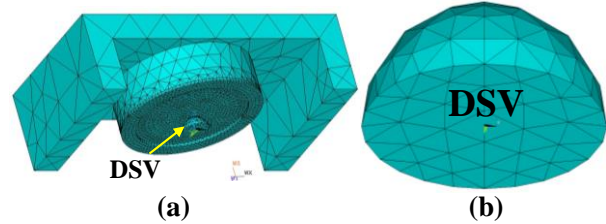


Fig. 5. 3D meshes of the model. (a) Magnet; (b) 60 mm DSV.

The FEM calculation takes into account the nonlinearity of the A3 steel yoke and the DT4 pure iron pole piece, the nonlinear relationships between  $B$  and  $H$  are shown in Fig. 6. Additionally, the relative permeability of the Nd-Fe-B (N40) permanent magnet is 1.085, and assumed a linear  $B$  vs.  $H$  dependence. This nonlinear electromagnetic problem is solved by the PSO algorithm (see the next section).

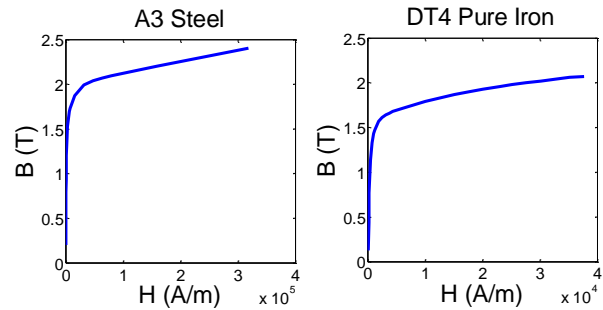


Fig. 6. Nonlinear magnetization curve of ferromagnetic materials used in the design: A3 steel and DT4 pure iron.

### D. Nonlinear optimization algorithm for the design of multi-ring pole pieces

The algorithm is programmed through MATLAB R2009b (Math Works, Natick, MA) and worked with ANSYS 14.0 for the magnetic field analysis. All the simulations were performed on a Dell computer with an Intel Core i7 CPU with 10 GB RAMS.

The flow of the optimization is shown in Fig. 7. Mathematically, the optimization can be expressed as:

$$\text{Minimize } y = f(H_i, S_i, D_j). \quad (3)$$

Subject to  $H_{min} \leq H_i \leq H_{max}$ ,  $S_{min} \leq S_i \leq S_{max}$ , and  $D_{min} \leq D_j \leq D_{max}$ , for  $i=1, \dots, 5$  and  $j=1, 2$ .

Where  $\Psi$  is the objective function;  $H_i$  is the height of the  $i$ th ring;  $S_i$  is the cross section width of the  $i$ th ring;

$D_j$  is the distance between two adjacent rings;  $H_i$ ,  $S_i$  and  $D_j$  are the design parameters whose elements are subject to the lower and upper limitations, respectively. The maximum number of rings we considered in our work is 5, meanwhile only these 16 kinds of multi-ring models shown in Fig. 4 are taken into consideration, so the value of  $i$  is 1,...,5, and the value of  $j$  is 1,2. We choose the uniformity of DSV as the objective function and the fitness of PSO defined by the formula:

$$\psi = \frac{B_{\max}(H_i, S_i, D_j) - B_{\min}(H_i, S_i, D_j)}{B_{\text{avg}}(H_i, S_i, D_j)} \times 10^6, \quad (4)$$

where  $B_{\min}$ ,  $B_{\max}$  are the maximum and the minimum nodal value for the magnetic flux density magnitude in the volume of 60 mm DSV, respectively, and  $B_{\text{avg}}$  is the average magnitude of the magnetic field flux density of the whole DSV.

Meanwhile, we take the magnitude of the magnetic field within the DSV into account, and a constraint should be added, that is,  $B_{\text{avg}} \geq 0.5$  T must be satisfied. Because the magnetic flux density of the magnet we design is 0.5T, which is mainly used for small animal imaging, meanwhile, the higher the magnetic flux density, the higher the image quality, and we set 0.5 T as the minimum requirement of the magnetic flux density.

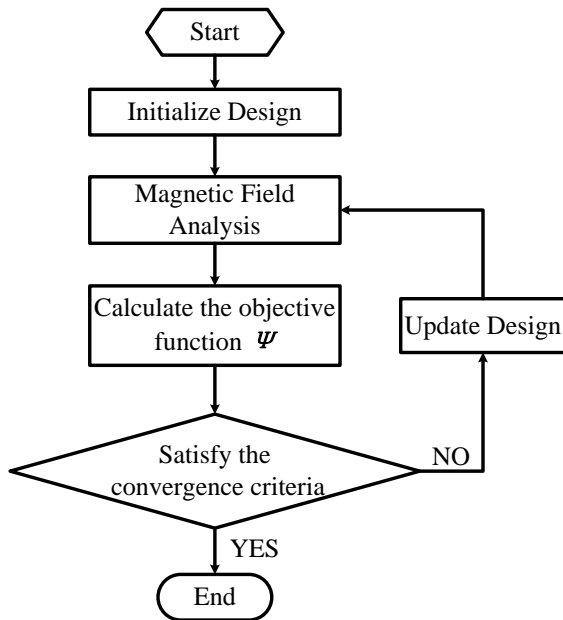


Fig. 7. The flow of the iterative optimization.

The design parameters are updated in the PSO based optimization procedure. Recent advances in the development of the PSO algorithm have elevated its capabilities in handling a wide class of complex engineering and science optimization problems [19-20].

Just as other evolutionary algorithms, the PSO algorithm searches solution using a swarm of particles that are updated from iteration to iteration. The flow of PSO is shown in Fig. 8. To find the best solution in the standard PSO algorithm, each particle changes its searching direction and position according to two factors, that is, its own best previous experience ( $pbest$ ) and the best experience of all other members ( $gbest$ ) according to the following equations which are proposed by Dr. Eberhart and Dr. Kennedy in 1995 [16]:

$$v_m^{k+1} = w v_m^k + c_1 rand() (pbest_m^k - x_m^k) + c_2 rand() (gbest^k - x_m^k), \quad (5)$$

$$x_m^{k+1} = x_m^k + v_m^{k+1}, \quad (6)$$

where  $k$  is the iteration index;  $v_m^k$  is the velocity of particle  $m$  at iteration  $k$  and  $x_m^k$  ( $x=H_i$ ,  $S_i$  and  $D_j$ ) is the current position of agent  $m$  at iteration  $k$ ;  $pbest_m^k$  is the best position of the particle  $m$  achieved based on its own experience and  $gbest^k$  is the best particle position based on overall swarm's experience;  $c_1$ ,  $c_2$  are two positive constants, and they are traditionally fixed to be 2;  $w$  is the inertial weight, which is between 0.5 and 1 [21] in this paper. After iterative updating by Equations (5) and (6), the global optimum can be found.

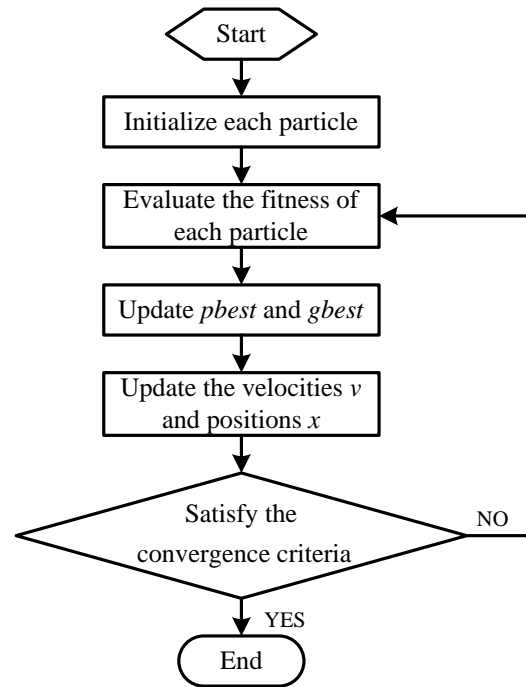


Fig. 8. The flow of PSO.

The iterative optimization process is repeated until a fixed number of iterations have been executed.

### III. RESULTS

After iterations of the nonlinear algorithm, the shapes of the pole piece are obtained through the

optimization of permutation and combination with several rings. The comparison of the flat pole piece, one shimming ring pole piece and the multi-ring pole pieces are tabulated in Table 1.

Table 1: Comparison of the magnetic field properties

Type	ID_Name	Magnetic Flux Density (T)	Uniformity (ppm)
No ring	NR	0.5815	609.51
One ring	1R	0.5270	51.28
Two ring	2R_1	0.5131	40.78
	2R_2	0.5312	35.72
Three ring	3R_1	0.5195	39.95
	3R_2	0.5130	34.82
	3R_3	0.5318	45.32
	3R_4	0.5308	40.17
Four ring	4R_1	0.5061	48.28
	4R_2	0.5195	44.55
	4R_3	0.5152	42.53
	4R_4	0.5139	43.06
	4R_5	0.5242	37.62
	4R_6	0.5327	48.53
Five ring	5R_1	0.5059	44.01
	5R_2	0.5103	49.94
	5R_3	0.5085	46.72
	5R_4	0.5235	42.16

Although the magnets with the optimized pole pieces, both one ring and multi-ring, weaken the magnetic flux density compared with the flat pole piece, they are all stronger than 0.5 T which satisfy the design requirement. Meanwhile, they all can significantly improve the magnetic field uniformity. Moreover, all multi-ring pole pieces we have designed in this paper produced the magnetic field uniformity better than the traditional one-ring pole piece named 1R. In all of the attempts, more rings with a little more complex structure can't make much better uniform magnetic field such as all five-ring cases which are inadvisable. But some of two and three-ring cases, such as 2R\_2 and 3R\_2, show an obvious improvement in terms of the uniformity of the magnetic field.

We chose the best three cases: 3R\_2, 2R\_2 and 4R\_5, which offered better field uniformities. The optimized parameters of the rings are displayed in Table 2. The cross-section and the 3D models of the three cases are compared to the traditional one-ring pole piece in Fig. 9.

The magnets with the optimized pole pieces maintain better density and uniformity of the magnetic field in different DSVs (diameters varied from 10mm-70mm) than the flat pole piece as shown in Fig. 10. These results can be used to estimate the magnetic flux density and uniformity inside the DSV.

From Table 1, we can see that the case of 3R\_2 has the minimum uniformity in a 60 mm DSV; however its magnetic flux density is the weakest among the best three cases, meanwhile, and it is also weaker than the traditional one-ring pole piece 1R, so it is inadvisable. The case of 4R\_5 can be taken into consideration, because it has a similar field density and a better field uniformity than the traditional one-ring pole piece 1R. The case 2R\_2 with a simple structure is acceptable, since its magnetic field is quite good in both the field density and uniformity.

Table 2: Optimized parameters of the best three cases

ID_Name	H <sub>i</sub> (mm)	S <sub>i</sub> (mm)	D <sub>j</sub> (mm)
3R_2	H <sub>1</sub> =14.23	S <sub>1</sub> =5.01	D <sub>1</sub> =9.53
	H <sub>2</sub> =6.74	S <sub>2</sub> =5.81	
	H <sub>3</sub> =10.49	S <sub>3</sub> =5.67	
2R_2	H <sub>1</sub> =9.90	S <sub>1</sub> =9.60,	D <sub>1</sub> =15.24
	H <sub>2</sub> =6.93	S <sub>2</sub> =6.74	
4R_5	H <sub>1</sub> =5.85	S <sub>1</sub> =4.58	D <sub>1</sub> =6.56
	H <sub>2</sub> =7.94	S <sub>2</sub> =5.49	
	H <sub>3</sub> =4.72	S <sub>3</sub> =5.97	
	H <sub>4</sub> =8.19	S <sub>4</sub> =5.78	

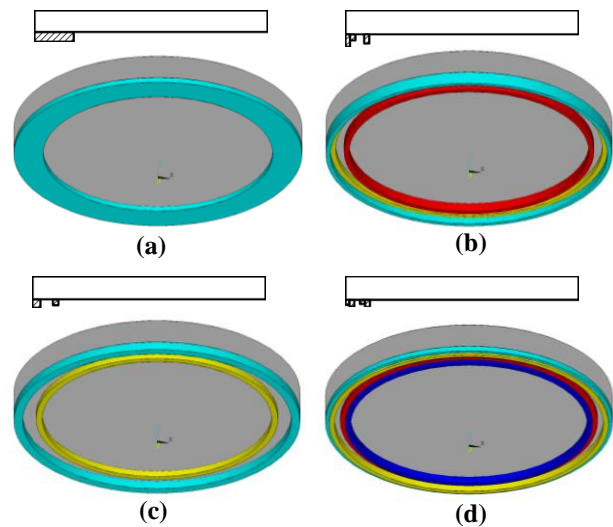


Fig. 9. The cross-section and 3D visualizations of the model. (a) 1R; (b) 3R\_2; (c) 2R\_2; (d) 4R\_5.

For the comparison of the traditional one-ring pole piece 1R and the case 2R\_2, the distributions of magnetic field of DSV are shown in Fig. 11. Figures 11 (a)-(b) represent the 1R case, and the scale of color bar is [0.526987 T, 0.527014 T] that the difference of the maximum and minimum is  $2.7 \times 10^{-5}$  T. Figures 11 (c)-(d) represent the case of 2R\_2, and the difference of the maximum and minimum is  $2.0 \times 10^{-5}$  T with the scale of color bar of [0.531162 T, 0.531182 T], which is smaller than the 1R case. The case 2R\_2 with a simple structure can provide a more uniform distribution of magnetic

field than the traditional one-ring pole piece.

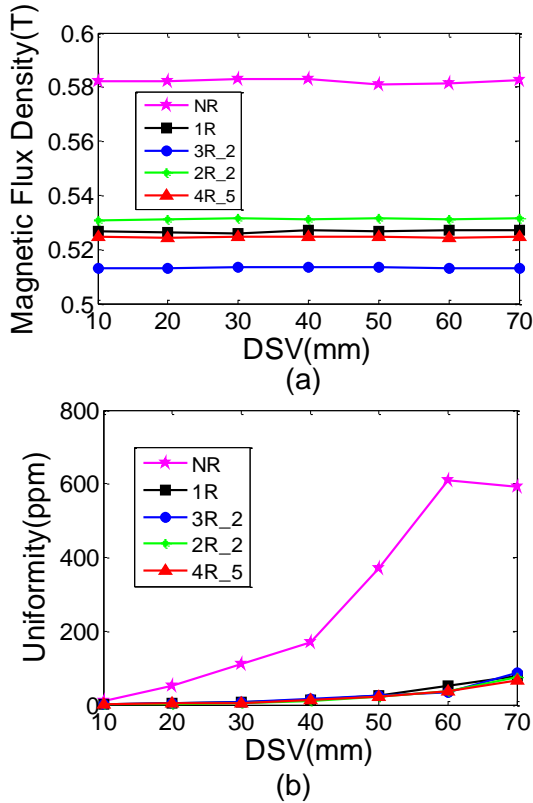


Fig. 10. Magnetic field with respect to the variation 10-70 mm of DSV. (a) Magnetic flux density; (b) uniformity.

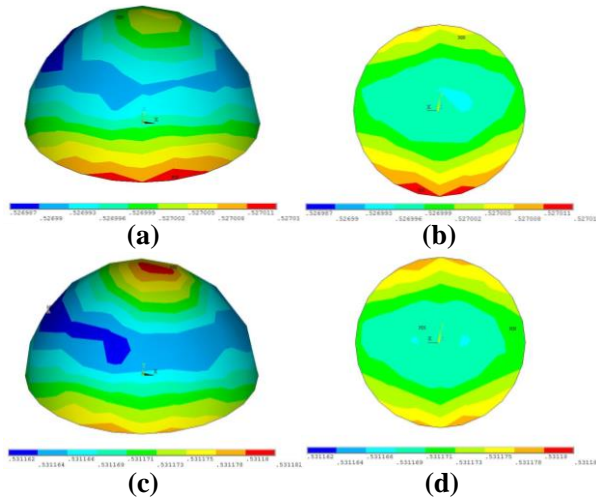


Fig. 11. Magnetic field distribution of DSV. (a) 1R: half DSV; (b) 1R:  $z=0$ ,  $xy$  plane; (c) 2R\_2: half DSV; (d) 2R\_2:  $z=0$ ,  $xy$  plane.

#### IV. CONCLUSION

In this paper, a nonlinear optimization and design of multi-ring pole pieces for a small-sized permanent MRI

magnet have been studied. A number of multi-ring pole piece configurations have been attempted, and the 3D FEM based simulation results demonstrate that, the proposed multi-ring pole piece can effectively improve the magnetic field uniformity. Compared with the traditional one-ring pole piece, the cases 2R\_2 and 4R\_5 both offer much better shimming solutions when there is no additional passive shim. Although larger number of rings such as five rings has a slightly better field uniformity than the one-ring pole piece, they are not desirable in practice, because it will increase the complexity of the shimming structure. The proposed shimming method can be effectively performed for various permanent MRI magnet systems. The scope of the theoretical work presented here can provide a reference to the actual magnet design and manufacture.

#### ACKNOWLEDGMENT

This work was supported in part by the National Natural Science Foundation of China under Grant No. 61701262, the scientific and technological project of Henan Province in China under Grant No. 182102310610, the key scientific research project in colleges of Henan Province in China under Grant No. 17A416005 & No. 17A510016 and the special project of Nanyang Normal University in China under Grant No. ZX2016011.

#### REFERENCES

- [1] Y. Zhang, D. Xie, B. Bai, H. S. Yoon, and C. S. Koh, "A novel optimal design method of passive shimming for permanent MRI magnet," *IEEE Trans. Magnetics*, vol. 44, pp. 1058-1061, 2008.
- [2] H. Sanchez Lopez, F. Liu, E. Weber, and S. Crozier, "Passive shim design and a shimming approach for biplanar permanent magnetic resonance imaging magnets," *IEEE Trans. Magnetics*, vol. 44, pp. 394-402, 2008.
- [3] J. Goebel, A. Pinzano, D. Grenier, A. Perrier, C. Henrionnet, L. Galois, P. Gillet, and O. Beuf, "New trends in MRI of cartilage: Advances and limitations in small animal studies," *Bio-medical Materials and Engineering*, vol. 20, pp. 189-194, 2010.
- [4] A. Schmid, J. Schmitz, J. Mannheim, F. Maier, K. Fuchs, H. Wehrl, and B. Pichler, "Feasibility of sequential PET/MRI using a state-of-the-art small animal PET and a 1 T benchtop MRI," *Molecular Imaging and Biology*, pp. 1-11, 2013.
- [5] T. Miyamoto, H. Sakurai, H. Takabayashi, and M. Aoki, "A development of a permanent magnet assembly for MRI devices using Nd-Fe-B material," *IEEE Trans. Magnetics*, vol. 25, pp. 3907-3909, 1989.
- [6] A. Momy and J. Taquin, "Low-leakage wide-access magnet for MRI," *IEEE Trans. Magnetics*, vol. 33, pp. 4572-4574, 1997.

- [7] C. Juchem, B. Muller-Bierl, F. Schick, N. Logothetis, and J. Pfeuffer, "Combined passive and active shimming for in vivo MR spectroscopy at high magnetic fields," *Journal of Magnetic Resonance*, vol. 183, pp. 278-289, 2006.
- [8] G. Sinha, R. Sundararaman, and G. Singh, "Design concepts of optimized MRI magnet," *IEEE Trans. Magnetics*, vol. 44, pp. 2351-2360, 2008.
- [9] X. Jiang, G. Shen, Y. Lai, and J. Tian, "Development of an open 0.3 T NdFeB MRI magnet," *IEEE Trans. Applied Superconductivity*, vol. 14, pp. 1621-1623, 2004.
- [10] A. Podol'skii, "Design procedure for permanent magnet assemblies with uniform magnetic fields for MRI devices," *IEEE Trans. Magnetics*, vol. 36, pp. 484-490, 2000.
- [11] A. Podol'skii, "Development of permanent magnet assembly for MRI devices," *IEEE Trans. Magnetics*, vol. 34, pp. 248-252, 1998.
- [12] D. Kim, B. Kim, J. Lee, W. Nah, and I. Park, "3-D optimal shape design of ferromagnetic pole in MRI magnet of open permanent-magnet type," *IEEE Trans. Applied Superconductivity*, vol. 12, pp. 1467-1470, 2002.
- [13] T. Tadic and B. G. Fallone, "Three-dimensional nonaxisymmetric pole piece shape optimization for biplanar permanent-magnet MRI systems," *IEEE Trans. Magnetics*, vol. 47, pp. 231-238, 2011.
- [14] T. Tadic and B. Fallone, "Design and optimization of a novel bored biplanar permanent-magnet assembly for hybrid magnetic resonance imaging systems," *IEEE Trans. Magnetics*, vol. 46, pp. 4052-4058, 2010.
- [15] J. Lee and J. Yoo, "Topology optimization of the permanent magnet type MRI considering the magnetic field homogeneity," *Journal of Magnetism and Magnetic Materials*, vol. 322, pp. 1651-1654, 2010.
- [16] J. Kennedy and R. Eberhart, "Particle swarm optimization," *IEEE International Conference of Neural Networks*, Perth, Australia, pp. 1942-1948, 1995.
- [17] Y. del Valle, G. Venayagamoorthy, S. Mohagheghi, J. Hernandez, and R. Harley, "Particle swarm optimization: Basic concepts, variants and applications in power systems," *IEEE Trans. Evolutionary Computation*, vol. 12, pp. 171-195, 2008.
- [18] J. Robinson and Y. Rahmat-Samii, "Particle swarm optimization in electromagnetics," *IEEE Trans. Antennas and Propagation*, vol. 52, pp. 397-407, 2004.
- [19] M. AlRashidi and M. El-Hawary, "A survey of particle swarm optimization applications in electric power systems," *IEEE Trans. Evolutionary Computation*, vol. 13, pp. 913-918, 2009.
- [20] J. Park, Y. Jeong, J. Shin, and K. Lee, "An improved particle swarm optimization for non-convex economic dispatch problems," *IEEE Trans. Power Systems*, vol. 25, pp. 156-166, 2010.
- [21] R. Eberhart and Y. Shi, "Tracking and optimizing dynamic systems with particle swarms," *Proceedings of the 2001 Congress on Evolutionary Computation*, pp. 94-100, 2001.



**Yi-Yuan Cheng** was born in Henan, China, in 1985. She received her B.E. degree in Biomedical Engineering from South-Central University for Nationalities, Wuhan, China, in 2008, and received Ph.D. degree in Biomedical Engineering from Zhejiang University, Hangzhou, China, in 2015. She is currently working as a Lecturer in the Department of Mechanical and Electrical Engineering in Nanyang Normal University, Nanyang, China. Her main research interests include MRI, design and optimization of magnet, artificial intelligence and so on.



**Tao Hai** was born in Henan, China, in 1974. He received his Ph.D. degree in Signal and Information Processing from Harbin Engineering University, Harbin, China. He is currently working as a Lecturer in the Department of Mechanical and Electrical Engineering in Nanyang Normal University, Nanyang, China. His main research interests include signal processing, image processing and so on.



**Yang-Bing Zheng** was born in Henan, China, in 1981. She received her M.Sc. degree in Detection Technology from China University of Geosciences (Wuhan), Wuhan, China, in 2008, and Ph.D. degree in Detection Technology and Automatic Equipment from China University of Mining and Technology (Beijing), Beijing, China, in 2014. She is currently working as a Lecturer in the Department of Mechanical and Electrical Engineering in Nanyang Normal University, Nanyang, China. Her main research interests include automatic control technology, intelligent instrument and so on.



**Bao-Lei Li** was born in Henan, China, in 1987. He received his Ph.D. degree in Information and Communication Engineering from Yunnan University, Kunming, China. He is currently working as a Lecturer in the Department of Physics and Electrical Engineering in Nanyang Normal University, Nanyang, China. His main research interests include intelligent optimization algorithm, path planning and so on.



**Ling Xia** was born in Zhejiang, China, in 1965. He received his B.E. degree in Automation and Ph.D. degree in Biomedical Engineering from Zhejiang University, Hangzhou, China. He is currently working as a Professor in the Department of Biomedical Engineering in Zhejiang University, Hangzhou, China. His main research interests include MRI key technical issues, biological effects of electromagnetic fields, Physiological simulation and modeling and so on.